Comput. Methods Appl. Mech. Engrg. 198 (2009) 1985–1995

Contents lists available at ScienceDirect

Comput. Methods Appl. Mech. Engrg.

journal homepage: www.elsevier.com/locate/cma

Solving elliptic problems with non-Gaussian spatially-dependent random coefficients

Xiaoliang Wan, George Em Karniadakis *

Division of Applied Mathematics, Brown University, Providence, RI 02912, USA

ARTICLE INFO

Article history:
Received 7 March 2008
Received in revised form 19 September 2008
Accepted 31 December 2008
Available online 24 January 2009

Keywords:
Polynomial chaos method
Monte Carlo method
Elliptic partial differential equation
Karhunen–Loève expansion
Uncertainty quantification

ABSTRACT

We propose a simple and effective numerical procedure for solving elliptic problems with non-Gaussian random coefficients, assuming that samples of the non-Gaussian random inputs are available from a statistical model. Given a correlation function, the Karhunen–Loève (K–L) expansion is employed to reduce the dimensionality of random inputs. Using the kernel density estimation technique, we obtain the marginal probability density functions (PDFs) of the random variables in the K–L expansion, based on which we define an auxiliary joint PDF. We then implement the generalized polynomial chaos (gPC) method via a collocation projection according to the auxiliary joint PDF. Based on the observation that the solution has an analytic extension in the parametric space, we ensure that the polynomial interpolation achieves *point-wise* convergence in the parametric space regardless of the PDF, where the energy norm is employed in the physical space. Hence, we can sample the gPC solution using the joint PDF instead of the auxiliary one to obtain the correct statistics. We also implement Monte Carlo methods to further refine the statistics using the gPC solution for variance reduction. Numerical results are presented to demonstrate the efficiency of the proposed approach.

1. Introduction

Uncertainty quantification has recently received a lot of attention with many classical deterministic mathematical models being reformulated in the stochastic sense. For example, physical parameters and boundary/initial conditions can be modeled by a random process instead of a deterministic function in the mean sense. In engineering applications, random inputs are often assumed to be Gaussian both for simplicity and by the virtue of the central limit theorem. However, the Gaussian assumption is not always valid since observation data exhibit distinct non-Gaussian characteristics in many cases. Thus, the simulation of non-Gaussian processes is of great practical importance. Although simulations of Gaussian processes are well established, simulations of non-Gaussian processes are still limited and actively under development. The main difficulty lies in the characterization of the random processes: unlike Gaussian processes which are determined solely through the first- and second-order probabilistic characteristics, one must know the entire family of joint distributions, which is never available in practice, for the non-Gaussian random processes.

At present, simulations of non-Gaussian processes are mainly based on memoryless nonlinear transforms of the standard Gaussian process due to the analytical tractability and availability of Gaussian simulation methods (spectral representation [1], Karhunen–Loève expansion [2], Wavelet expansion [3], and Fourier–Wavelet expansion [4], etc.). Recent attempts utilize the Hermite polynomial chaos method [5,6] by expressing a non-Gaussian process $R(t)$ as

$$R(t) = \sum_{i=1}^{\infty} a_i H_i(G(t)),$$

where H_i is the Hermite polynomial of degree i, and $G(t)$ is a standard one-dimensional stationary Gaussian process. In [7], the Karhunen–Loève expansion was employed to simulate non-Gaussian processes.

All these simulation methods can be coupled directly with Monte Carlo methods to simulate the random response of the system. However, due to the low convergence rate, brute-force Monte Carlo methods are usually not affordable in large-scale simulations. Thus, acceleration techniques for Monte Carlo methods and non-statistical approaches have been developed. One such non-statistical approach is polynomial chaos, which is a spectral expansion of a given random function with respect to a multi-dimensional random variable. In literature, polynomial chaos is often coupled with the K–L expansion of the random inputs (see [8–15] and references therein). If the random inputs can be expressed by a standard Gaussian process, the polynomial chaos (Hermite-chaos) method can be employed directly to capture the

* Corresponding author.
E-mail address: gk@dam.brown.edu (G.E. Karniadakis).

0045-7825/$ - see front matter © 2009 Elsevier B.V. All rights reserved.
doi:10.1016/j.cma.2008.12.039

uncertainty propagation, since the random variables in the K–L expansion are *mutually independent*. However, the following situations can significantly weaken the effectiveness of polynomial chaos methods for non-Gaussian random inputs:

(i) A strongly non-Gaussian processes $R(t)$ may require a high-order polynomial chaos expansion with respect to $G(t)$. If $R(t)$ represents the random input, a high-order polynomial chaos expansion of the solution field may also be necessary for convergence, which may not be possible due to the limitation of high dimensionality and complexity.
(ii) When the K–L expansion is employed to simulate the non-Gaussian random processes, polynomial chaos or its extensions [9,10,13,15] cannot be used directly since all random variables in the K–L expansion are uncorrelated but not independent. If *independence* is assumed, the joint probability density between random variables cannot be captured.

In the present work, we study an elliptic problem with a random coefficient, which is a typical stochastic model in many physical applications, such as porous media, ground-water systems, etc. In particular, we re-examine the polynomial chaos methods coupled with the K–L expansion. However, we take into account the joint probability density of uncorrelated random variables in the K–L expansion. We treat the polynomial chaos method as a high-dimensional approximation approach, and take advantage of the property of the solution that it has an *analytic* extension in the parametric space. We observe that the polynomial chaos interpolation provides L_∞ convergence in the parametric space regardless of the joint PDF. Thus, the polynomial chaos solution can actually be regarded as a statistical model, based on which we can sample the joint PDF to obtain the desired statistics. Accordingly, we sample a known function instead of the original stochastic PDE, which results in substantial computational savings. Furthermore, we can also use the polynomial chaos solution as a control variate for variance reduction to sample the original stochastic PDE to efficiently refine the obtained statistics.

This paper is organized as follows: we first present some necessary techniques and analysis results for the model problem given in the next section. We then describe our methodology in Section 3. In Section 4, we analyze the convergence behavior of our methodology. A numerical study is given in Section 5, and we conclude in Section 6 with a brief discussion.

2. Model problem

Let $(\Omega, \mathscr{F}, P)$ be a complete probability space, where Ω is the sample space, $\mathscr{F}$ is the σ-algebra of subsets of Ω and P is a proper probability measure. Let D be a bounded, connected, open subset of $\mathbb{R}^d (d = 1, 2, 3)$ with a Lipschitz continuous boundary ∂D. We consider the following stochastic elliptic problem as a model problem: find a stochastic function, $u : \Omega \times \overline{D} \to \mathbb{R}$, such that almost surely (a.s.) the following equation holds:

$$\begin{aligned} &-\nabla \cdot (a(\boldsymbol{x};\omega)\nabla u(\boldsymbol{x};\omega)) = f(\boldsymbol{x}) \quad \text{on } D, \\ &u(\boldsymbol{x};\omega) = 0 \quad \text{on } \partial D, \end{aligned} \tag{1}$$

where $f(\boldsymbol{x})$ is assumed to be a deterministic function for simplicity, and $a(\boldsymbol{x};\omega)$ is a second-order random process satisfying the following strong ellipticity condition:

Assumption 2.1 (*Strong ellipticity condition*). Let $a(\boldsymbol{x};\omega) \in L_\infty(\overline{D};\Omega)$ be strictly positive with lower and upper bounds a_{min} and a_{max}, respectively,

$$0 < a_{min} < a_{max} \quad \text{and} \quad \Pr(a(\boldsymbol{x};\omega) \in [a_{min}, a_{max}] \quad \forall \boldsymbol{x} \in \overline{D}) = 1. \tag{2}$$

Remark 2.2. The strong ellipticity condition can be relaxed as: there exist a positive number $a_{\min} > 0$ such that $a(\boldsymbol{x};\omega) > a_{\min}$ almost surely [16]. In this work, we use the strong ellipticity assumption for the discussion of our methodology and present some numerical experiments for the more general cases.

2.1. High-dimensional deterministic problem

In practice, the most commonly used (non-Gaussian) random processes are second-order stationary processes with a known correlation function $K_a(\boldsymbol{x}_1, \boldsymbol{x}_2) = \mathbb{E}[(a(\boldsymbol{x}_1,\omega) - \mathbb{E}[a](\boldsymbol{x}_1))(a(\boldsymbol{x}_2,\omega) - \mathbb{E}[a](\boldsymbol{x}_2))]$. Based on the correlation function K_a, we can implement the K–L expansion in the form:

$$a(\boldsymbol{x};\omega) = \mathbb{E}[a](\boldsymbol{x}) + \sum_{i=1}^{\infty} \sqrt{\lambda_i} Y_i \psi_i(\boldsymbol{x}), \tag{3}$$

where $\{Y_i\}_{i=1}^{\infty}$ is a set of uncorrelated random variables with zero mean and unit variance, and $\{(\lambda_i, \psi_i(\boldsymbol{x}))\}_{i=0}^{\infty}$ is a set of eigenvalue–eigenfunction pairs satisfying

$$\int_D K_a(\boldsymbol{x}_1, \boldsymbol{x}_2)\psi_i(\boldsymbol{x}_2)\mathrm{d}\boldsymbol{x}_2 = \lambda_i \psi_i(\boldsymbol{x}_1), \tag{4a}$$

$$\int_D \psi_i(\boldsymbol{x})\psi_j(\boldsymbol{x})\mathrm{d}\boldsymbol{x} = \delta_{ij}, \tag{4b}$$

where δ_{ij} is the Kronecker symbol. Furthermore, the random variables Y_i satisfy

$$Y_i = \frac{1}{\sqrt{\lambda_i}} \int_D (a(\boldsymbol{x};\omega) - \mathbb{E}[a](\boldsymbol{x}))\psi_i(\boldsymbol{x})\mathrm{d}\boldsymbol{x}. \tag{5}$$

The eigenvalue problem (4), in general, does not have analytical solutions, which means that numerical approximation is usually necessary [17–19]. We note here that Y_i are uncorrelated, but *not necessarily independent*, for general (non-Gaussian) random inputs. For numerical implementation, we need to truncate the K–L expansion up to M terms as

$$a_M(\boldsymbol{x};\omega) = \mathbb{E}[a](\boldsymbol{x}) + \sum_{i=1}^{M} \sqrt{\lambda_i} Y_i \psi_i(\boldsymbol{x}) \tag{6}$$

according to the L_2 convergence

$$\mathbb{E}\left[\int_D (a(\boldsymbol{x};\omega) - a_M(\boldsymbol{x};\omega))^2 \mathrm{d}\boldsymbol{x}\right] = \sum_{i>M} \lambda_i \to 0 \quad \text{as } M \to \infty. \tag{7}$$

It is known that the K–L expansion is optimal in the L_2 sense. We rewrite the problem (1) as

$$\begin{aligned} &-\nabla \cdot (a_M(\boldsymbol{x};\boldsymbol{Y})\nabla u(\boldsymbol{x};\boldsymbol{Y})) = f(\boldsymbol{x}) \quad \text{on } D, \\ &u(\boldsymbol{x};\boldsymbol{Y}) = 0 \quad \text{on } \partial D, \end{aligned} \tag{8}$$

where $\boldsymbol{Y} = (Y_1, \ldots, Y_M)$ is a multi-dimensional random variable. Then the solution $u(\boldsymbol{x};\boldsymbol{Y})$ will be determined by a finite number of random variables Y_i according to the Doob–Dynkin lemma [20]. Due to the strong ellipticity condition, we see that $\boldsymbol{Y}$ must be bounded. From Eq. (5), we have

$$|Y_i| \leqslant \frac{a_{\max} - a_{\min}}{\sqrt{\lambda_i}} \int_D |\psi_i(\boldsymbol{x})|\mathrm{d}\boldsymbol{x} \leqslant \frac{(a_{\max} - a_{\min})\mathrm{Vol}(D)}{\sqrt{\lambda_i}}.$$

Without loss of generality, we can assume that $\boldsymbol{Y} \in \Gamma = \prod_{i=1}^{M} \Gamma_i$, and $\Gamma \in \mathbb{R}^M$ is compact. We denote $r_i = \sqrt{\lambda_i}\|\psi_i(\boldsymbol{x})\|_{L_\infty(D)}$, $i = 1, \ldots, M$. It is obvious that the value of M is determined by the decay rate of eigenvalues λ_i, which, in general, relies on the regularity of the correlation function $K_a(\boldsymbol{x}_1, \boldsymbol{x}_2)$. For more discussions about the decay rate of λ_i we refer to [13].

2.2. Density estimation

In this section, we present algorithms for the density estimation, which are necessary for our methodology in Section 3. In practice, it is impossible to obtain the joint PDF of Y_i. However, we can approximate the marginal PDFs ρ_i of Y_i efficiently using density estimation approaches. Here we employ the technique of kernel density estimator [21]. Given N_ρ realizations of the random field $a(\boldsymbol{x};\omega)$, we can obtain a set $\{Y_i^{(j)}\}_{j=1}^{N_\rho}$ of samples for Y_i using Eq. (5). Then the kernel density estimation $\tilde{\rho}_i$ of ρ_i takes the form

$$\tilde{\rho}_i = \frac{1}{N_\rho h}\sum_{j=1}^{N_\rho} K_d\left(\frac{y_i - Y_i^{(j)}}{h}\right), \tag{9}$$

where $h > 0$ is the bandwidth acting as a tuning parameter and $K_d(y)$ is a prescribed kernel function satisfying

$$K_d(y) \geqslant 0, \quad \int_{\mathbb{R}} K_d(y)\mathrm{d}y = 1.$$

The most widely used kernel is the Gaussian kernel $K_d(y) = (2\pi)^{1/2}\mathrm{e}^{-y^2/2}$. In this case, the kernel density estimate can be written as

$$\tilde{\rho}_i = \frac{1}{N_\rho h\sqrt{2\pi}}\sum_{j=1}^{N_\rho} \mathrm{e}^{-(y_i - Y_i^{(j)})^2/2h^2}. \tag{10}$$

The bandwidth h is a scaling factor, which determines the quality of the approximate marginal PDF $\tilde{\rho}_i$. To this end, we choose the optimal bandwidth h, which minimizes the *asymptotic integrated mean square error* (AIMSE). In particular, AIMSE represents the distance between two density functions, which can be written as

$$\mathrm{AIMSE}(\tilde{\rho}_i, \rho_i) = \frac{1}{N_\rho h}\int_{\mathbb{R}} K_d^2\mathrm{d}y + \frac{1}{4}h^4\int_{\mathbb{R}} y^2 K_d(y)\mathrm{d}y\int_{\mathbb{R}}(\rho_i'')^2\mathrm{d}y,$$

with ρ_i'' being the second-order derivative of ρ_i, see [22,23] and the references therein for more details about numerical algorithms of non-parametric density estimation. The best rate of convergence of the AIMSE of the kernel density estimation is of order $O(N_\rho^{-4/5})$ [22,23].

2.3. L_∞ approximation of $u(\boldsymbol{x},\boldsymbol{y})$

In this section, we discuss briefly the gPC method via a collocation projection, or gPC interpolation in short. The regularity of the solution $u(\boldsymbol{x};\boldsymbol{y})$ in the parametric space $\boldsymbol{y} \in \Gamma$ was given in the following lemma [16]:

Lemma 2.3. *Let* $\Gamma_i^* = \prod_{j=1, j\neq i}^{M}\Gamma_j$ *and* $\boldsymbol{y}^{i,*} \in \Gamma_i^*$, $i = 1,\ldots,M$. *Let* $\gamma_i = r_i/a_{min}$. *The solution* $u(\boldsymbol{x};y_i,\boldsymbol{y}^{i,*},\boldsymbol{x})$ *admits an analytic extension* $u(\boldsymbol{x};z,\boldsymbol{y}^{i,*})$, $z \in \mathbb{C}$, *in the region of the complex plane*

$$\Sigma(\Gamma_i;\tau_i) \equiv \{z \in \mathbb{C}, \mathrm{dist}(z,\Gamma_i) \leqslant \tau_i\}$$

with $0 < \tau_i < 1/(2\gamma_i)$. *Furthermore,*

$$\max_{z\in\Sigma(\Gamma_i;\tau_i)} \|u(z)\|_{H_0^1(D)} \leqslant C(\tau_i,\gamma_i,a_{\min}),$$

where C *is function of* τ_i, γ_i *and* $a_{\min}$.

Due to the analyticity, we are interested in the point-wise convergence of polynomial interpolation in the parametric space. In particular, we will examine gPC interpolation based on sparse grids. In this section we assume that the random variables Y_i are independent for discussions about gPC interpolation and return to this issue later in Section 3.

Let $\mathscr{P}_p(\Gamma)$ indicate polynomials on Γ with the total polynomial order up to p. We define an approximation space for the model problem (8) as $\mathscr{P}_p(\Gamma)\otimes H_0^1(D)$, where we do not include the errors from physical discretization for simplicity. An interpolation operator based on sparse grids can be defined as

$$\mathscr{I}_p v = v \quad \forall v \in \mathscr{P}_p(\Gamma)\otimes H_0^1(D). \tag{11}$$

We note that $\mathscr{P}_p(\Gamma)$ is usually not the same as the polynomial space that polynomial interpolation on sparse grids can exactly produce. If we use $\mathscr{A}(M+s,M)$ to indicate the tensor product formulas given by the Smolyak algorithm, where s indicates the level of sparseness, polynomial interpolation based on $\mathscr{A}(M+s,M)$ will be exact for polynomials in $\mathscr{P}_s(\Gamma)$ and some other polynomials with a degree larger than s [24]. However, in this work we will focus on the part $\mathscr{P}_s(\Gamma)$.

Given a set of sparse grids $\{\boldsymbol{y}_i\}_{i=1}^n$ on Γ, we compute $u(\boldsymbol{x};\boldsymbol{y}_i)$ by solving the deterministic elliptic equation

$$-\nabla\cdot(a_M(\boldsymbol{x};\boldsymbol{y}_i)\nabla u(\boldsymbol{x};\boldsymbol{y}_i)) = f(\boldsymbol{x}), \tag{12}$$

where the number n of interpolation points is large enough to exactly determine polynomials up to order p on Γ. When necessary, we project the gPC interpolation results onto a basis of $\mathscr{P}_p(\Gamma)$ through the discrete integration formula based on sparse grids. We note that if $\mathscr{A}(M+p,M)$ is based on Gauss abscissas, the corresponding discrete integration formula has a degree of exactness $2p+1$ for $p < 2M$ [25], i.e., the discrete integration formula will be exact for polynomials with an order up to $2p+1$.

To this end, the point-wise error of the gPC interpolation via sparse grids can be expressed as

$$\|u - \tilde{u}_p\|_{L_\infty(\Gamma;H_0^1(D))} \leqslant (\Lambda_n + 1)\inf_{w\in\mathscr{P}_p(\Gamma)\otimes H_0^1(D)}\|u + w\|_{L_\infty(\Gamma;H_0^1(D))}, \tag{13}$$

where $\tilde{u}_p = \mathscr{I}_p u$ and Λ_n is the Lebesgue constant associated with the collocation points $\{\boldsymbol{y}_i\}_{i=1}^n$. It is obvious that the convergence is controlled by two factors: the Lebesgue constant and the best approximation given by the polynomial space $\mathscr{P}_p(\Gamma)$. Due to the existence of analytic extension in the parametric space, we know that the best approximation has a fast (exponential) point-wise convergence [26]. However, the Lebesgue constant is only understood well for certain choices of collocation points, e.g., Jacobi nodes. For a one-dimensional interpolation formula, the optimal order of the Lebesgue constant is $\log(m+1)$ with m being the polynomial order [24]. Polynomial interpolation on sparse grids was studied in [27], where the sparse grids were based on the extrema of the Chebyshev polynomials. Although the authors considered functions in a Sobolev-type space, the deviations can be directly applied to analytic functions, due to the special tensor-product structure of Smolyak algorithm, for an estimate of point-wise convergence. Regarding the stochastic collocation finite element method for the model problem (8), the $L_2(\Gamma;H_0^1(D))$ approximation was studied in [16,28], and the $L_\infty(\Gamma;H_0^1(D))$ approximation was analyzed in [29], where sparse collocation points were generated by a full tensor product with anisotropic Chebyshev nodes in each random dimension, and the random variables Y_i were assumed to be mutually independent.

In this work, we will employ sparse grids based on Gauss abscissas for an arbitrary PDF, which is in general a Jacobi-like function (see Fig. 4 in Section 5). Since we know that it is possible to use the Jacobi nodes to get the optimal order $\log(m+1)$ for the Lebesgue constant through the "additional points method" [24], we expect a fast point-wise convergence for the right-hand side of Eq. (13). In this work, we just use the Gauss abscissas for a Jacobi-like PDF, and numerical experiments show that the corresponding sparse grids work well for the gPC interpolation with respect to the $L_\infty(\Gamma;H_0^1(D))$ norm.

Remark 2.4. In the polynomial interpolation, the PDF of $\boldsymbol{Y}$ does not affect the norm $\|\cdot\|_{L_\infty(\Gamma;H_0^1(D))}$ directly unlike the L_2 norm, which means that the point-wise convergence is valid for any joint PDF of Y_i. However, we note that the PDF of $\boldsymbol{Y}$ can be implicitly related to

the choice of grid points $\{\boldsymbol{y}_i\}$, which will affect the Lebesgue constant.

Remark 2.5. For the Galerkin projection, the $L_\infty(\Gamma; H_0^1(D))$ convergence of the polynomial approximation should also be valid due to the analytic extension in the parametric space. To study the L_∞ convergence, the standard technique is to transfer the problem to the approximation of Green's functions of the adjoint problem. To the best of our knowledge, no regularity study of such Green's functions is available yet. In this work, we will present some numerical experiments based on the Galerkin projection results.

Based on the point-wise convergence in the parametric space, we are now ready to describe our methodology for elliptic problems with general (non-Gaussian) random inputs.

3. Proposed methodology

The model problem (8) has been widely studied (see [30,9,31,12,13,16,28,32] and references therein) using the polynomial chaos method, where the uncorrelated random variables in the K–L expansion of $a(\boldsymbol{x};\omega)$ are either approximated by a set of independent Gaussian random variables or just assumed to be mutually independent. In this work, we take advantage of the point-wise convergence of polynomial interpolation in the parametric space to develop a simple and effective methodology.

3.1. Approximation procedure

Let $\tilde{a}(\boldsymbol{x};\omega) = \mathscr{S}a(\boldsymbol{x};\omega)$ denote a simulator of $a(\boldsymbol{x};\omega)$. For example, $\mathscr{S}$ can be a statistical model or a numerical simulation algorithm of the non-Gaussian random process $a(\boldsymbol{x};\omega)$ [5–7]. In other words, we can obtain samples of the random field $a(\boldsymbol{x};\omega)$ from the simulator $\mathscr{S}$, based on which we can implement a direct Monte Carlo method. Since brute-force Monte Carlo methods are usually unaffordable, especially for large-scale simulations, we shall try to accelerate it by employing polynomial chaos simulations.

Since the K–L expansion is valid for any second-order stationary or non-stationary random process, we use it to reduce the number of random dimensions, i.e.,

$$\tilde{a}_M(\boldsymbol{x};\omega) = \mathbb{E}[\tilde{a}](\boldsymbol{x}) + \sum_{i=1}^{M} \sqrt{\lambda_i} Y_i \psi_i(\boldsymbol{x}), \tag{14}$$

where the random variable Y_i is defined as

$$Y_i = \frac{1}{\sqrt{\lambda_i}} \int_D (\tilde{a}(\boldsymbol{x};\omega) - \mathbb{E}[\tilde{a}](\boldsymbol{x}))\psi_i(\boldsymbol{x})\mathrm{d}\boldsymbol{x}. \tag{15}$$

Then, the marginal PDF ρ_i of Y_i can be approximated by density estimation (see Section 2.2) using Eq. (15). Based on the approximate marginal PDFs $\tilde{\rho}_i$, we subsequently define an auxiliary PDF $\tilde{\rho} = \prod_{i=1}^{M} \tilde{\rho}_i$. In other words, *independence* is assumed between Y_i although they are only mutually uncorrelated. The reason in defining $\tilde{\rho}$ is to construct orthogonal (generalized) polynomial chaos bases $\{\phi_\alpha\}$ and the corresponding Gauss quadrature points for $\boldsymbol{Y} = (Y_1, \ldots, Y_M) \in \Gamma$ with respect to the marginal PDFs $\tilde{\rho}_i$, based on which we generate sparse grids in the parametric space. Here $\alpha = (\alpha_1, \ldots, \alpha_M) \in \mathbb{N}_0^M$ is a multi-index. $\{\phi_\alpha\}$ is a set of orthogonal polynomials with respect to the auxiliary PDF $\tilde{\rho}$, where $\phi_\alpha = \prod_{i=1}^{M} \phi_{\alpha_i}$ and $\{\phi_{\alpha_i}\}$ is a set of orthogonal polynomials with respect to the marginal PDF $\tilde{\rho}_i$. Several issues must be clarified before we try to obtain orthogonal polynomial chaos basis $\{\phi_\alpha\}$:

(1) The image of $\boldsymbol{Y}$ is usually hard to obtain in practice. However, the marginal PDF ρ_i usually decay fast as $|Y_i|$ becomes large. We then truncate the image of Y_i at a certain point where $\tilde{\rho}_i$ is relatively small and obtain $\boldsymbol{Y} \in \widetilde{\Gamma} \subset \Gamma$. Thus, we neglect $\boldsymbol{Y} \in \Gamma \setminus \widetilde{\Gamma}$, since the probability $\Pr(\boldsymbol{Y} \in \Gamma \setminus \widetilde{\Gamma})$ is very small.

(2) To obtain orthogonal polynomials corresponding to the marginal PDF ρ_i, we need to construct them numerically [15]. The efficiency of algorithms for numerical orthogonality is mainly affected by the smoothness of the marginal PDF ρ_i [33]. Thus, we need an algorithm which can give us a smooth approximation of ρ_i. We noted in Section 2.2 that the smoothness of the approximate marginal PDF $\tilde{\rho}_i$ is inherited from the smoothness of the kernel K_d. If the Gaussian kernel is employed, we have $\tilde{\rho}_i \in C^\infty(\Gamma_i)$. Thus $\tilde{\rho}_i$ is proper for the algorithms of numerical orthogonality. From Eq. (9), we can see that the cost for the evaluation of $\tilde{\rho}_i$ at a given point is determined by the number N_ρ of samples. If N_ρ is large, the cost for numerical orthogonality is large. However, we note that $\tilde{\rho}_i$ is nothing more but a sum of a series of Gaussian functions, which implies that the fast Gauss transform (FGT) [34,19] can be employed to accelerate the calculation. Actually, numerical experiments show that the cost for numerical orthogonality is very small. In general, the interpolation error of $\mathscr{I}_p u$ is not very sensitive to the accuracy of $\tilde{\rho}_i$, see Section 5 for a convergence study.

Using the polynomial chaos basis $\{\phi_\alpha\}$ with order $|\alpha| = \sum_{i=1}^{M} \alpha_i \leqslant p$, we can model the solution field as

$$\tilde{u}_p(\boldsymbol{x};\boldsymbol{Y}) = \sum_{|\alpha| \leqslant p} \tilde{u}_\alpha(\boldsymbol{x})\phi_\alpha(\boldsymbol{Y}), \tag{16}$$

where the coefficients $\tilde{u}_\alpha$ can be obtained from the interpolation results $u(\boldsymbol{x};\boldsymbol{y}_i)$

$$\tilde{u}_\alpha(\boldsymbol{x}) = \sum_{i=1}^{n} u(\boldsymbol{x};\boldsymbol{y}_i)\phi_\alpha(\boldsymbol{y}_i)w_i, \tag{17}$$

with w_i being the associated integration weight of grid $\boldsymbol{y}_i$. We note here that the discrete Galerkin projection is based on the auxiliary PDF $\tilde{\rho}$ instead of the joint PDF of $\boldsymbol{Y}$.

3.2. Post-processing procedure

Since the polynomial approximation $\tilde{u}_p(\boldsymbol{x};\boldsymbol{Y})$ is based on the auxiliary PDF $\tilde{\rho}$ while all the statistics of $u(\boldsymbol{x};\boldsymbol{Y})$ are with respect to the joint PDF ρ, we must deal with the approximation $\tilde{u}_p(\boldsymbol{x};\boldsymbol{Y})$ carefully to obtain the correct statistics. Since the gPC interpolation $\tilde{u}_p(\boldsymbol{x};\boldsymbol{Y})$ has a point-wise convergence in the parametric space, we known the statistics of $\tilde{u}_p(\boldsymbol{x};\boldsymbol{Y})$ with respect to the joint PDF of $\boldsymbol{Y}$ should converge to the statistics of $u(\boldsymbol{x};\boldsymbol{Y})$. Based on such an observation, we propose two post-processing models:

(i) *GPC predictor model: although* we do not have the explicit form of the joint PDF, we can sample it using the simulator $\mathscr{S}$. We first obtain a sample field of $\tilde{a}(\boldsymbol{x};\omega)$ from the simulator $\mathscr{S}$, and then compute samples of Y_i using Eq. (15). Then, the moments of $u(\boldsymbol{x};\boldsymbol{Y})$ can be obtained as

$$\mathbb{E}[u^m(\boldsymbol{x};\tilde{a}(\boldsymbol{x}))] \approx \frac{1}{N_{mc}} \sum_{i=1}^{N_{mc}} B_u^m(\boldsymbol{x};\boldsymbol{Y}^{(i)}), \tag{18}$$

where

$$B_u(\boldsymbol{x};\boldsymbol{Y}^{(i)}) = \begin{cases} \tilde{u}_p(\boldsymbol{x};\boldsymbol{Y}^{(i)}) & \text{if } \boldsymbol{Y}^{(i)} \in \Gamma, \\ 0 & \text{otherwise} \end{cases}$$

and N_{mc} is the number of realizations. In other words, we sample the polynomial chaos solution $\tilde{u}_p(\boldsymbol{x};\boldsymbol{Y})$ instead of the stochastic elliptic PDE. If the polynomial chaos solution

provides a good point-wise approximation, we will obtain a good speed-up since sampling the stochastic PDE directly is much more expensive.

(ii) *GPC predictor–corrector model: furthermore,* using the polynomial chaos solution as a control variate for *variance reduction*, we can further refine the results obtained from the first model. We implement the Monte Carlo method to sample the stochastic PDE in the following way:

$$\mathbb{E}[u^m(\boldsymbol{x};\tilde{a}(\boldsymbol{x}))] = \mathbb{E}[\tilde{u}_p^m(\boldsymbol{x};\boldsymbol{Y})] + \frac{1}{N_{mc}}\sum_{i=1}^{N_{mc}}[u^m(\boldsymbol{x};\boldsymbol{Y}^{(i)}) - B_u^m(\boldsymbol{x};\boldsymbol{Y}^{(i)})], \tag{19}$$

where $\mathbb{E}[\tilde{u}_p^m(\boldsymbol{x};\boldsymbol{Y})]$ is computed from the joint PDF instead of the auxiliary PDF, and $B_u(\boldsymbol{x},\boldsymbol{Y}^{(i)})$ is defined as in Eq. (18). Since we have the explicit form of $\tilde{u}_p(\boldsymbol{x};\boldsymbol{Y})$, we can use a large number of samples to compute $\mathbb{E}[\tilde{u}_p^m(\boldsymbol{x};\boldsymbol{Y})]$ accurately. If $\tilde{u}_p^m(\boldsymbol{x};\boldsymbol{Y})$ is a good approximation of $u^m(\boldsymbol{x};\boldsymbol{Y})$, the random variable $u^m(\boldsymbol{x};\boldsymbol{Y}) - B_u^m(\boldsymbol{x};\boldsymbol{Y})$ will have a small variance and result in a good variance reduction for the Monte Carlo method, see Section 4 about the error analysis. In other words, the value of N_{mc} can be reduced significantly to achieve convergence.

We now summarize our algorithm:

1: ***Compute*** marginal PDFs $\tilde{\rho}_i$ of uncorrelated random variables Y_i in the K–L expansion by sampling the simulator $\mathscr{S}$ of random inputs.
2: ***Generate*** orthogonal polynomial chaos basis for each marginal PDF $\tilde{\rho}_i$.
3: ***Construct*** orthogonal multi-dimensional orthogonal polynomial chaos basis for the auxiliary PDF $\tilde{\rho} = \prod_{i=1}^{M}\tilde{\rho}_i$.
4: ***Implement*** the polynomial chaos method via the collocation or Galerkin projection to obtain the approximation $u(\boldsymbol{x},\boldsymbol{y}_i)$ on $\{\boldsymbol{y}_i\}_{i=1}^n \subset \Gamma$ based on the auxiliary PDF $\tilde{\rho}$.
5: ***Project*** the interpolation results from step 4 onto the polynomial chaos basis $\{\phi_\alpha\}$ to obtain the chaos expansion $\tilde{u}_p(\boldsymbol{x};\boldsymbol{Y})$.
6: ***Compute*** statistics by sampling the polynomial chaos approximation $\tilde{u}_p(\boldsymbol{x};\boldsymbol{Y})$ as in Eq. (18) or use it as a control variate for variance reduction as in Eq. (19).

4. Error analysis of the proposed methodology

In this section we present a general error analysis for the methodology proposed in Section 3. We first list the main error sources:

(1) Truncation of the marginal PDFs. In numerical implementation, we cannot exactly obtain the image Γ of $\boldsymbol{Y}$. Instead we use a truncated version $\tilde{\Gamma} \subset \Gamma$.
(2) Approximation of $\tilde{u}_p(\boldsymbol{x};\boldsymbol{Y}) = \mathscr{I}_p u$ based on the auxiliary PDF.

Lemma 4.1. *We assume that*

$$\int_{\tilde{\Gamma}^c} \|u\|_{H_0^1(D)}^2 \rho(\boldsymbol{y})\mathrm{d}\boldsymbol{y} \leqslant \epsilon_1^2 \quad \text{and} \quad \|u(\boldsymbol{x};\boldsymbol{y}) - \tilde{u}_p(\boldsymbol{x};\boldsymbol{y})\|_{L_\infty(\tilde{\Gamma};H_0^1(D))} \leqslant \epsilon_2,$$

where $\tilde{\Gamma}^c = \Gamma \setminus \tilde{\Gamma}$, and $\rho(\boldsymbol{y})$ is the joint PDF of $\boldsymbol{Y}$. Then we have

$$|\mathbb{E}[\|u\|_{H_0^1(D)}] - \mathbb{E}[\|\tilde{u}_p\|_{H_0^1(D)}]| \leqslant \epsilon_1 + \epsilon_2. \tag{20}$$

Proof.

$$\begin{aligned}
&|\mathbb{E}[\|u\|_{H_0^1(D)}] - \mathbb{E}[\|\tilde{u}_p\|_{H_0^1(D)}]| \\
&\leqslant \mathbb{E}[|\|u\|_{H_0^1(D)} - \|\tilde{u}_p\|_{H_0^1(D)}|] \\
&\leqslant \mathbb{E}[\|u - \tilde{u}_p\|_{H_0^1(D)}] \\
&= \int_{\tilde{\Gamma}^c} \|u\|_{H_0^1(D)}\rho(\boldsymbol{y})\mathrm{d}\boldsymbol{y} + \int_{\tilde{\Gamma}} \|u - \tilde{u}_p\|_{H_0^1(D)}\rho(\boldsymbol{y})\mathrm{d}\boldsymbol{y} \\
&\leqslant \left(\int_{\tilde{\Gamma}^c} \|u\|_{H_0^1(D)}^2\rho(\boldsymbol{y})\mathrm{d}\boldsymbol{y}\right)^{1/2}\left(\int_{\tilde{\Gamma}^c}\rho(\boldsymbol{y})\mathrm{d}\boldsymbol{y}\right)^{1/2} \\
&\quad \text{(Cauchy—Schwarz inequality)} \\
&\quad + \int_{\tilde{\Gamma}} \|u - \tilde{u}_p\|_{H_0^1(D)}\rho(\boldsymbol{y})\mathrm{d}\boldsymbol{y} \\
&\leqslant \epsilon_1 + \epsilon_2.
\end{aligned}$$

It is seen that ϵ_1 is due to the truncation of image of $\boldsymbol{Y}$. The error of $\tilde{u}_p$ with respect to the joint PDF $\rho(\boldsymbol{y})$ is dominated by the L_∞ error ϵ_2 given by the approximation with respect to the auxiliary PDF.

Remark 4.2. The assumption that $\int_{\tilde{\Gamma}^c}\|u\|_{H_0^1(D)}^2\rho(\boldsymbol{y})\mathrm{d}\boldsymbol{y} \leqslant \epsilon_1^2$ is reasonable since $u(\boldsymbol{x};\boldsymbol{Y}) \in L_2(\Gamma;H_0^1(D))$ [31].

Lemma 4.3. *Let*

$$u_H = \mathbb{E}[\|\tilde{u}_p\|_{H_0^1(D)}] + \frac{1}{N_{mc}}\sum_{i=1}^{N_{mc}}\left[\|u\|_{H_0^1(D)}(\boldsymbol{Y}^{(i)}) - \|B_u\|_{H_0^1(D)}(\boldsymbol{Y}^{(i)})\right],$$

where $\boldsymbol{Y}^{(i)}$ are samples from the simulator of random inputs, and $B_u(\boldsymbol{x},\boldsymbol{Y}^{(i)})$ is defined as in Eq. (18). We have the convergence estimate

$$|\mathbb{E}[u] - u_H| \sim O\left(\sqrt{\epsilon_1^2 + \epsilon_2^2}N_{mc}^{-1/2}\right). \tag{21}$$

Proof. We examine the variance of $d_u = \|u\|_{H_0^1(D)} - \|B_u\|_{H_0^1(D)}$.

$$\begin{aligned}
\mathrm{Var}(d_u) &= \mathbb{E}[d_u^2] - (\mathbb{E}[d_u])^2 \leqslant \mathbb{E}[(\|u\|_{H_0^1(D)} - \|B_u\|_{H_0^1(D)})^2] \\
&\leqslant \int_{\tilde{\Gamma}^c}\|u\|_{H_0^1(D)}^2\rho(\boldsymbol{y})\mathrm{d}\boldsymbol{y} + \int_{\tilde{\Gamma}}\|u - \tilde{u}_p\|_{H_0^1(D)}^2\rho(\boldsymbol{y})\mathrm{d}\boldsymbol{y} \leqslant \epsilon_1^2 + \epsilon_2^2.
\end{aligned}$$

Thus, $u_H = \mathbb{E}[\|\tilde{u}_p\|_{H_0^1(D)}] + \mathbb{E}[\|u\|_{H_0^1(D)}] - \mathbb{E}[\|\tilde{u}_p\|_{H_0^1(D)}] + O\left(\sqrt{\epsilon_1^2 + \epsilon_2^2}N_{mc}^{-1/2}\right)$, where we use the convergence rate of Monte Carlo methods.

Remark 4.4. From Lemma 4.3 we see that the efficiency of the polynomial chaos solution for variance reduction is determined by the error ϵ_1 and ϵ_2. In Lemma 4.3 we assume that $\mathbb{E}[\|\tilde{u}_p\|_{H_0^1(D)}]$ is exactly known. In practice, it is possible that we can only obtain $\mathbb{E}[\|\tilde{u}_p\|_{H_0^1(D)}]$ by sampling the random inputs. However, since $\tilde{u}_p$ is an explicit polynomial, it will be much faster to obtain a desired accuracy compared to sampling the stochastic PDE.

Remark 4.5. One option to reduce the errors ϵ_1 and ϵ_2 is the multi-element extension of polynomial chaos methods [14,15], where the parametric space is decomposed for extra *h*-type convergence. In fact, by doing the decomposition, the domain of analytic extension will be also enlarged, see [35] for more details.

5. Numerical studies

5.1. Algebraic model

We first investigate the convergence of the proposed methodology using a simple algebraic problem

$$(c + \sigma(\xi_1 + \xi_2))u = 1, \tag{22}$$

where c and σ are positive numbers, and ξ_i, $i = 1,2$ are two *uncorrelated* random variables. For solvability, we assume that $\xi_1 \in [-1,1]$ and $c + \sigma(\xi_1 + \xi_2) > 0$.

For simplicity, we assume that $\xi_2 = \xi_2(\xi_1)$ is a function of ξ_1. Then the fact that ξ_1 and ξ_2 are uncorrelated implies orthogonality between ξ_1 and ξ_2 with respect to the PDF $f(\xi_1)$ of ξ_1. In other words, ξ_2 can be expressed as an orthogonal polynomial of ξ_1. We note that ξ_2 is dependent on ξ_1. In the phase space, (ξ_1, ξ_2) is located on a curve $\xi_2 = \xi_2(\xi_1)$; however, if we use the auxiliary PDF $\rho(\xi_1, \xi_2)$, (ξ_1, ξ_2) is on $[-1, 1]^2$. This can be regarded as the worst case for our methodology since we need to approximate a one-dimensional problem using two-dimensional polynomials. It is obvious that the convergence on $[-1, 1]^2$ in the L_2 norm is not enough for the convergence on the curve $\xi_2(\xi_1)$. A stronger metric to measure the convergence of polynomial chaos is needed, such as the L_∞ norm.

Following the methodology proposed in Section 3, we first sample ξ_1 and ξ_2 to obtain the density estimation. Based on the estimated marginal PDFs we construct orthogonal polynomials and implement the gPC method. Finally, we compute the statistics using the joint PDF, in other words, we sample ξ_1 since we know that ξ_2 is a function of ξ_1.

Let ξ_1 be a Beta random variable of distribution Beta $(\frac{1}{2},\frac{1}{2})$. We let $\xi_2 = 2\xi_1^2 - 1$. It is easy to verify that ξ_2 also has a Beta distribution Beta $(\frac{1}{2},\frac{1}{2})$. We have two choices for constructing the polynomial chaos basis corresponding to the auxiliary joint PDF.

(i) Construct the two-dimensional polynomial chaos basis using the one-dimensional Chebyshev polynomials since both marginal PDFs of ξ_1 and ξ_2 are Beta $(\frac{1}{2},\frac{1}{2})$.

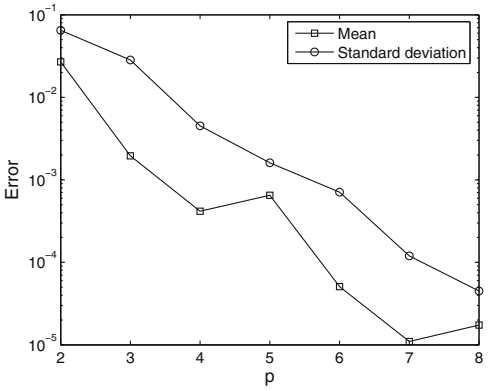

Fig. 1. Convergence of the mean and standard deviation for the algebraic model. Chebyshev polynomials are used to construct the polynomial chaos basis corresponding to the auxiliary PDF.

(ii) Estimate the marginal PDFs of ξ_1 and ξ_2, and then construct orthogonal polynomial chaos basis numerically.

Both cases are investigated. In Fig. 1 we show the convergence of mean and standard deviation for approach (i). All statistics are computed with respect to the joint PDF $\delta(\xi_2 - \xi_2(\xi_1))\rho_{(\frac{1}{2},\frac{1}{2})}(\xi_1)$, where $\rho_{(\frac{1}{2},\frac{1}{2})}(\cdot)$ is the PDF of $B(\frac{1}{2},\frac{1}{2})$ distribution. It can be seen that the overall convergence rate is, in fact, exponential. If we use the solutions from approach (ii) and the joint PDF $\delta(\xi_2 - \xi_2(\xi_1))\rho_{(\frac{1}{2},\frac{1}{2})}(\xi_1)$ to compute the desired statistics, we also obtain fast (exponential) convergence, as shown in Fig. 2. It can be seen that the convergence behavior is similar for $N_\rho = 100$ and $100,000$. In Fig. 3, we present some estimated marginal PDFs and demonstrate the sensitivity of convergence with respect to the sample size for density estimation. It is observed that the estimated marginal PDFs may be very different, however, the corresponding approximation errors can be of the same order. In other words, convergence is not sensitive to the sample size for density estimation. The reason is that the solution of the algebraic model is analytic with respect to ξ_1 and ξ_2, and the Taylor expansion converges in the L_∞ norm.

5.2. One-dimensional elliptic model

In this section we study the performance of the proposed methodology numerically using an one-dimensional elliptic problem

$$-\frac{\mathrm{d}}{\mathrm{d}x}\left(a(x;\omega)\frac{\mathrm{d}u(x;\omega)}{\mathrm{d}x}\right) = 1, \quad x \in (0,1)$$
$$u(x;\omega) = 0, \quad x = 0, 1, \tag{23}$$

where the random process $a(x;\omega)$ takes the form

$$a(x;\omega) = \mathrm{e}^{G(x;\omega)} \tag{24}$$

and $G(x;\omega)$ is a Gaussian random process of zero mean satisfying an exponential kernel.

5.2.1. The Karhunen–Loève expansion of $a(x;\omega)$

Let $K_G(x_1, x_2)$ denote the covariance kernel of $G(x)$ with the form

$$K_G(x_1, x_2) = \sigma^2 \mathrm{e}^{-|x_1 - x_2|/l}, \tag{25}$$

where σ is constant and l the correlation length. We know that the K–L expansion of $G(x;\omega)$ is

$$G(x;\omega) = \sigma \sum_{i=1}^{\infty} \sqrt{\lambda_{G,i}} h_{G,i}(x) Z_i, \tag{26}$$

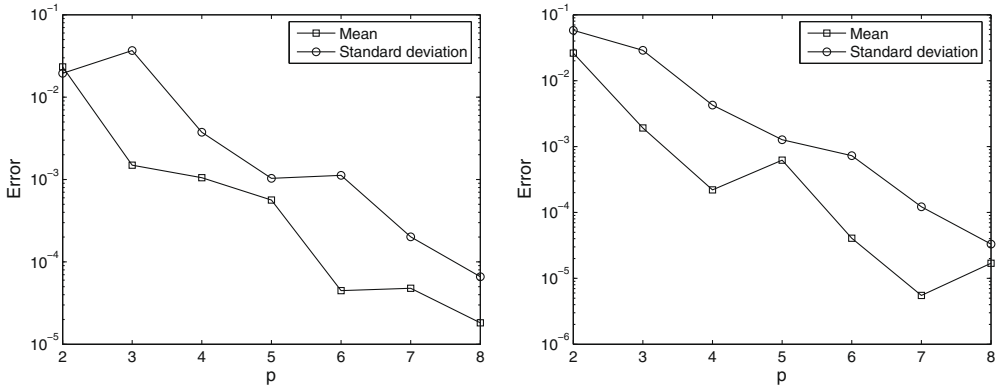

Fig. 2. Convergence of the mean and standard deviation for the algebraic model. Estimated marginal PDFs are used for the numerical orthogonality. Left: 100 samples for density estimation. Right: 100,000 samples for density estimation.

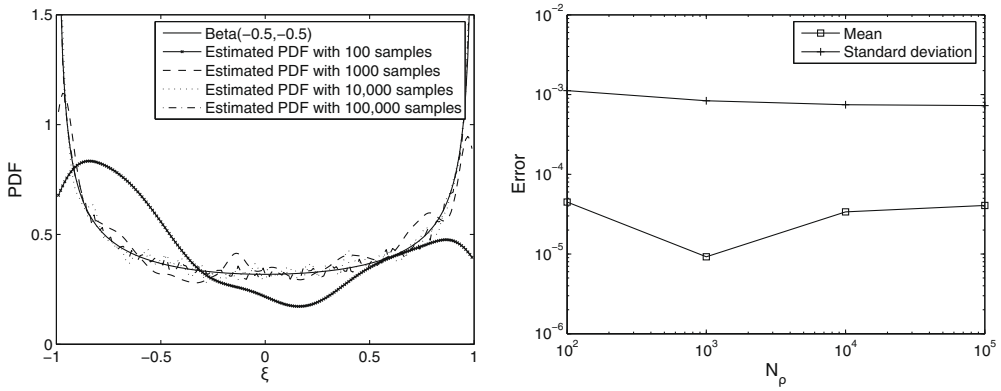

Fig. 3. Left: PDF of Beta $(\frac{1}{2},\frac{1}{2})$ and estimated ones with different numbers of samples. Right: sensitivity of numerical convergence with respect to the sample size in the density estimation.

where $\{\lambda_{G,i}, h_{G,i}\}_{i=1}^{\infty}$ are eigenpairs and $\{Z_i\}$ is a set of independent random variables with zero mean and unit variance. We obtain the following statistics of $a(x;\omega)$:

- Mean:

$$\bar{a}(x) = \mathbb{E}[a] = \mathrm{e}^{\frac{1}{2}\sigma^2}.$$

- Variance:

$$\mathrm{Var}(a) = \mathbb{E}[(a-\bar{a})^2] = \mathrm{e}^{2\sigma^2} - \mathrm{e}^{\sigma^2}.$$

- Correlation function:

$$K_a(x_1,x_2) = \frac{\mathbb{E}[(a(x_1;\omega)-\bar{a}(x_1))(a(x_2;\omega)-\bar{a}(x_2))]}{\mathrm{Var}(a)} = \frac{\mathrm{e}^{\sigma^2\mathrm{e}^{-|x_1-x_2|/l}} - 1}{\mathrm{e}^{\sigma^2}-1}.$$

The K–L expansion of $a(x;\omega)$ takes the form

$$a_M(x;\omega) = \bar{a}(x) + \sigma_a \sum_{i=1}^{M} \sqrt{\lambda_{a,i}} h_{a,i}(x) Y_i. \tag{27}$$

We note that Y_i are *not* independent.

5.2.2. Numerical orthogonality

For the underlying Gaussian random process, we let $\sigma = 0.3$ and $l = 5$. Using Eq. (15), we can obtain the marginal PDFs of random variables Y_i in the K–L expansion of the random process $a(x;\omega)$. In Fig. 4, the estimated marginal PDFs of Y_i are shown. For comparison, we include the normal distribution. It can be seen that the marginal PDFs of Y_i are different from the normal distribution. There exists an apparent bias in the marginal PDF of Y_1 towards the negative direction. We note that all the estimated PDFs are smooth.

In Fig. 5 we present some orthogonal polynomials with respect to the marginal PDFs of Y_1 and Y_2. It is seen that nonsymmetric structure in the marginal PDFs is clearly reflected in the orthogonal polynomials, in particular, the fifth-order polynomials.

5.2.3. Convergence of the proposed strategy

Due to the absence of exact solutions, we use the solutions given by Monte Carlo simulations as reference solutions.

Let $\tilde{u}_p(x;\boldsymbol{Y})$ be the polynomial chaos approximation of $u(x;\omega)$ based on the auxiliary PDF $\tilde{\rho}$. For this example, we compute $\tilde{u}_p(x;\boldsymbol{Y})$ through the gPC method via the Galerkin projection. Let N_ρ indicate the size of samples for marginal density estimation and N_{mc} the number of realizations for Monte Carlo simulation. We approximate the statistics of solution using the following four methods:

(i) Implement Monte Carlo simulations with 10^5 realizations.
(ii) Sample $\tilde{u}_p(x;\boldsymbol{Y})$ with respect to the auxiliary PDF $\tilde{\rho}$. We note that this method is only correct when the random variables in the K–L expansion of $a(x;\omega)$ are independent, otherwise, there exists a model error in the random inputs.
(iii) Sample $\tilde{u}_p(x;\boldsymbol{Y})$ with respect to the joint PDF ρ using the gPC predictor model, see Eq. (18).

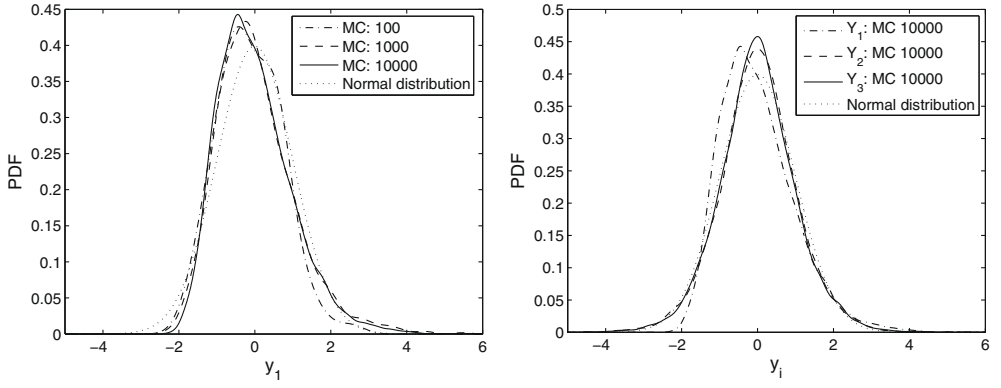

Fig. 4. Estimated marginal PDFs using different numbers of sample points. Right: PDFs of Y_i, $i = 1,2,3$.

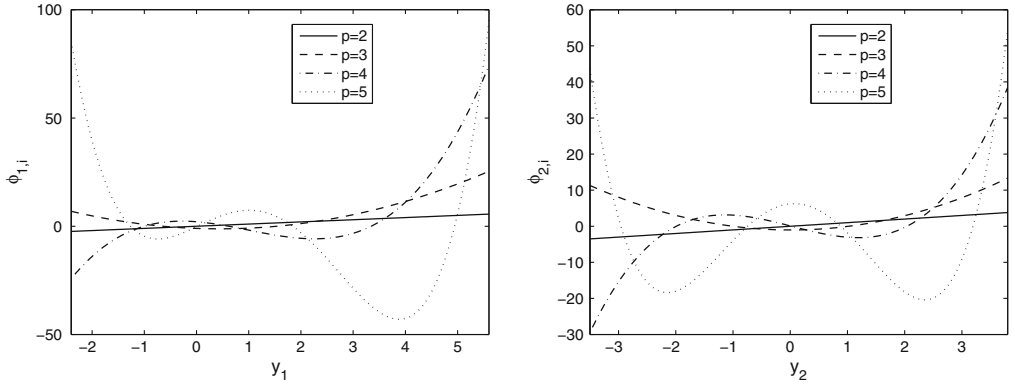

Fig. 5. Orthogonal polynomials with polynomial order $p = 2, \ldots, 5$ with respect to the estimated marginal PDFs. Left: $\phi_{1,i}(y_1)$. Right: $\phi_{2,i}(y_2)$

(iv) Implement Monte Carlo simulations using the gPC predictor–corrector model, see Eq. (19).

For the underlying Gaussian random process, we let $\sigma = 0.2$ and $l = 5$. For this case, the eigenvalues decay fast and we keep the first five eigenvalues for the K–L expansion of the log-normal process $a(x;\omega)$. We use a 20-term K–L expansion to approximate the underlying Gaussian process $G(x;\omega)$ when Monte Carlo simulations are needed.

In Fig. 6 we show the mean and standard deviation of $u(x;\omega)$ given by the first three methods. It is seen that the results are close to each other, which implies that the correlation between Y_i has a small effect on the statistics up to second order due to the Gaussian-like marginal PDFs.

We subsequently investigate the convergence of methods (iii) and (iv). Let $Q_{\text{ref}}(x)$ be a reference function and $Q(x)$ an approximation. We define the difference between Q and Q_{ref} as

$$\epsilon = \frac{|Q(x) - Q_{\text{ref}}(x)|}{\max\limits_{0 \leqslant x \leqslant 1} |Q_{\text{ref}}(x)|}. \tag{28}$$

We use the results given by Monte Carlo simulations with 10^5 realizations as a reference. In Fig. 7 we show the convergence behavior with respect to ϵ for different polynomial orders p and sample size N_ρ used in the kernel density estimation. For the mean, it is clear that ϵ becomes smaller as the sample size N_ρ for the density estimation increases. Similar behavior is observed for the standard deviation. However, the error ϵ of the standard deviation given by

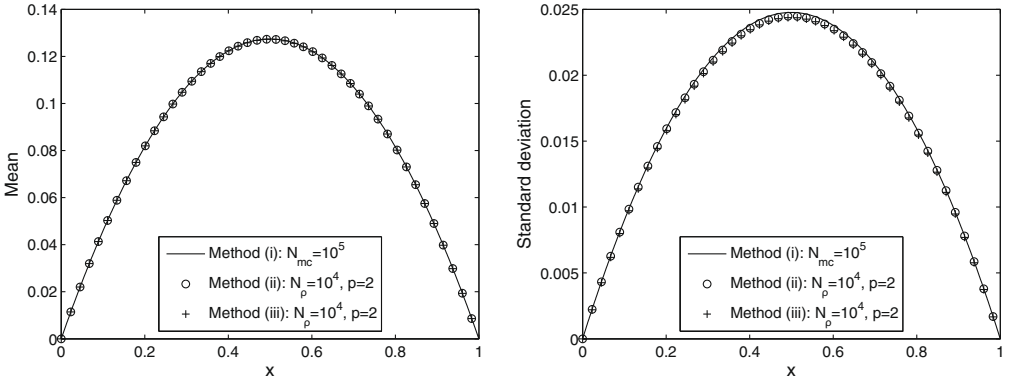

Fig. 6. Mean and standard deviation of $u(x;\omega)$ given by different methods. Five-term K–L expansion of $a(x;\omega)$. Left: mean. Right: standard deviation.

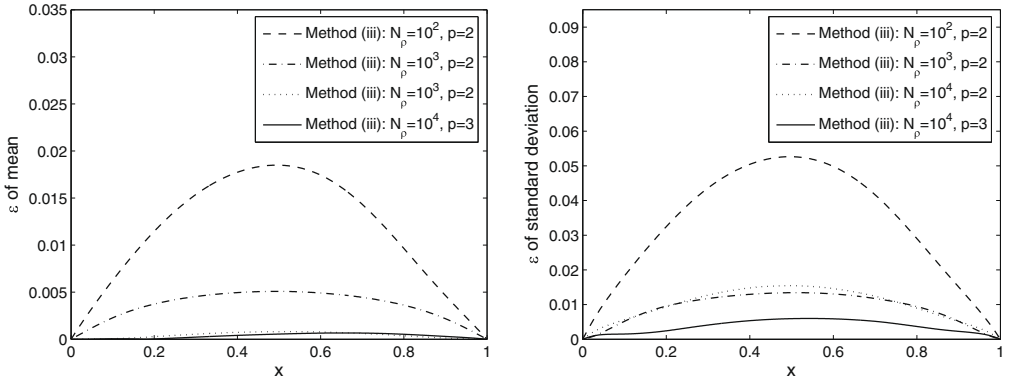

Fig. 7. Difference of statistics between the proposed strategy and Monte Carlo simulations. Five-term K–L expansion of $a(x;\omega)$ is employed. Left: mean. Right: standard deviation.

$N_\rho = 10^3$ is almost the same as that given by $N_\rho = 10^4$ when $p = 2$. Then we increase the polynomial order to $p = 3$ and obtain a smaller ϵ, which implies that the error from polynomial chaos is dominant for $p = 2$ and $N_\rho = 10^3, 10^4$. Thus, the proposed strategy converges to the correct results when N_ρ and p increase. In contrary to the algebraic model, we see that the size of samples for density estimation has noticeable influence on the convergence. This is because the long tails of PDFs can be approximated better if a larger number of samples is used, in other words, the error ϵ_1 in Lemma 4.1 is reduced.

However, when the number of random dimensions is large, it is not efficient to increase the polynomial order. Thus, it is necessary to consider the method (iv). We compare the results from methods (iii) and (iv) in Fig. 8. It is seen that a small number of realizations of the stochastic elliptic problems can significantly improve the convergence, which implies that the polynomial chaos solution based on the auxiliary PDF provides a good prediction for variance reduction, in other words, the factor $\sqrt{\epsilon_1^2 + \epsilon_2^2}$ in Lemma 4.3 is small.

5.3. Two-dimensional elliptic model

Let $G_i(\boldsymbol{x};\omega)$, $i = 1, 2, \ldots, 2m$ be independent Gaussian random fields with zero mean and unit variance, where m is a positive integer. Each Gaussian random field has the same correlation function $K_G(\boldsymbol{x}_1, \boldsymbol{x}_2) = K_G(|\boldsymbol{x}_1 - \boldsymbol{x}_2|)$. We consider the following nonnegative random field:

$$R_\Gamma(\boldsymbol{x};\omega) = \frac{1}{2}\sum_{i=1}^{2m} G_i^2(\boldsymbol{x};\omega). \tag{29}$$

It can be verified that given $\boldsymbol{x}$, the marginal distribution of $R_\Gamma(\boldsymbol{x};\omega)$ is a gamma distribution of mean m. Therefore, $R_\Gamma(\boldsymbol{x};\omega)$ can be called a homogeneous Gamma random field. We summarize the statistics of $R_\Gamma(\boldsymbol{x};\omega)$ as follows

- Mean:

$$\overline{R}_\Gamma = \mathbb{E}[R_\Gamma] = m.$$

- Variance:

$$\mathrm{Var}(R_\Gamma) = \mathbb{E}[(R_\Gamma - \overline{R}_\Gamma)^2] = m.$$

- Correlation function:

$$K_{R_\Gamma}(\boldsymbol{x}_1, \boldsymbol{x}_2) = \frac{\mathbb{E}[(R_\Gamma(\boldsymbol{x}_1;\omega) - \overline{R}_\Gamma(\boldsymbol{x}_1))(R_\Gamma(\boldsymbol{x}_2;\omega) - \overline{R}_\Gamma(\boldsymbol{x}_2))]}{\mathrm{Var}(R_\Gamma)} = K_G^2(\boldsymbol{x}_1, \boldsymbol{x}_2).$$

The derivation of the correlation function is given in Appendix A. We see that the correlation function of $R_\Gamma(\boldsymbol{x};\omega)$ is *independent* of m.

We consider the following non-Gaussian coefficient

$$a(\boldsymbol{x};\omega) = 1 + \sigma R_\Gamma(\boldsymbol{x};\omega) \tag{30}$$

for the model problem (1). Based on the K–L expansions of the underlying Gaussian fields $G_i(\boldsymbol{x};\omega)$, $a(\boldsymbol{x};\omega)$ can be approximated as

$$a(\boldsymbol{x};\omega) \approx \hat{a}(\boldsymbol{x};\{\xi_{i,j}\}) = 1 + \frac{\sigma}{2}\sum_{i=1}^{2m}\left(\sum_{j=1}^{M}\lambda_{G,j}h_{G,j}(\boldsymbol{x})\xi_{i,j}\right)^2, \tag{31}$$

where $\xi_{i,j}$ are independent standard Gaussian random variables.

To employ the standard procedure of polynomial chaos methods, we need to project the approximate Gamma field $\hat{a}(\boldsymbol{x},\{\xi_{i,j}\})$ onto Hermite-chaos. However, we notice there are several issues related to the efficiency of polynomial chaos methods: (1) the number of random variables is mM, which increases fast with respect to m; (2) second-order Hermite-chaos is necessary to represent the random inputs, which implies that high-order Hermite-chaos may be necessary to model the solution.

In contrast to the standard procedure, we start from the correlation function of $R_\Gamma(\boldsymbol{x};\omega)$, which has a simple relation with the correlation function $K_G(\boldsymbol{x}_1, \boldsymbol{x}_2)$ and is independent of the number of underlying Gaussian random fields. We assume that $K_G(\boldsymbol{x}_1, \boldsymbol{x}_2)$ is a Gaussian kernel as

$$K_G(\boldsymbol{x}_1, \boldsymbol{x}_2) = \mathrm{e}^{-\frac{|\boldsymbol{x}_1 - \boldsymbol{x}_2|^2}{l}}. \tag{32}$$

Then the correlation function of $R_\Gamma(\boldsymbol{x};\omega)$ is

$$K_{R_\Gamma}(\boldsymbol{x}_1, \boldsymbol{x}_2) = \mathrm{e}^{-\frac{|\boldsymbol{x}_1 - \boldsymbol{x}_2|^2}{l/2}}. \tag{33}$$

It is seen that the correlation function of $R_\Gamma(\boldsymbol{x};\omega)$ is also Gaussian with a half correlation length compared to $K_G(\boldsymbol{x}_1, \boldsymbol{x}_2)$. The K–L expansion of $a(\boldsymbol{x};\omega)$ can be expressed as

$$a(\boldsymbol{x};\omega) = 1 + \sigma\left(\mathbb{E}[R_\Gamma] + \mathrm{std}(R_\Gamma)\sum_{i=1}^{\infty}\sqrt{\lambda_i}h_i(\boldsymbol{x})Y_i\right) = 1 + \sigma m + \sigma m^{1/2}\sum_{i=1}^{\infty}\sqrt{\lambda_i}h_i(\boldsymbol{x})Y_i, \tag{34}$$

where $\mathrm{std}(R_\Gamma)$ is the standard deviation of $R_\Gamma(\boldsymbol{x})$, $\{\lambda_i, h_i(\boldsymbol{x})\}_{i=1}^{\infty}$ is a set of eigenpairs of $K_{R_\Gamma}(\boldsymbol{x}_1, \boldsymbol{x}_2)$, and $\{Y_i\}$ is set of mutually uncorrelated random variables with zero mean and unit variance. Given a realization of $a(\boldsymbol{x};\omega)$, a sample of Y_i can be obtained as

$$Y_i = \frac{1}{\sigma m^{1/2}\sqrt{\lambda_i}}\int_D (a(\boldsymbol{x}) - (1+\sigma)m)h_i(\boldsymbol{x})\mathrm{d}\boldsymbol{x}. \tag{35}$$

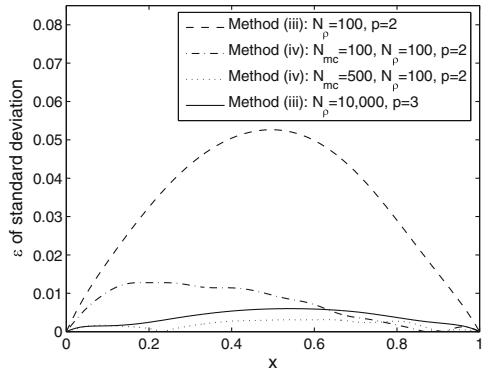

Fig. 8. Accelerate Monte Carlo simulations using the polynomial chaos approximation for variance reduction.

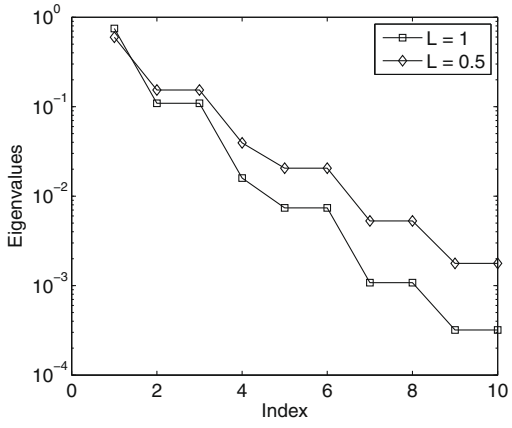

Fig. 9. Eigenvalues of Gaussian covariance kernels with correlation length $l = 1, 0.5$.

In numerical approximation, we obtain realizations of $a(\boldsymbol{x};\omega)$ through a set of independent Gaussian random variables using Eq. (31). For a good accuracy, we let $M = 30$.

For this example, we consider the gPC method via a collocation projection. Let the physical domain $D = (0,1)^2$, $f(\boldsymbol{x}) = 1$, and $\sigma = 0.2$. Let the correlation length $l = 1$ for the underlying Gaussian random fields, which yields that the correlation length for the corresponding Gamma random field is $l/2 = 0.5$. In Fig. 9, we show the first 10 largest eigenvalues of Gaussian kernels with $l = 1, 0.5$. It can be seen that we need $M = 4$ Gaussian random variables to keep 90% energy in the K–L expansion of $G_i(\boldsymbol{x};\omega)$. Consider $m = 20$. If the standard procedure is employed, we need $mM = 80$ independent Gaussian random variables to approximate the Gamma random field. For the gPC interpolation, 2,342,921 grid points are needed for non-nested sparse grids with sparseness level 3 based on the one-dimensional Gauss quadrature formula. The choice of sparseness level 3 is according to the fact that the second-order Hermite-chaos approximation is needed for the random inputs. However, if we implement the K–L expansion directly with respect to the correlation function of $R_\Gamma(\boldsymbol{x};\omega)$, only 8 mutually uncorrelated random variables are necessary to keep 99% energy. In contrast to the standard procedure, the dimension of random inputs is dramatically reduced. In this work, we keep the first 10 eigenvalues of $K_{R_\Gamma}(\boldsymbol{x}_1,\boldsymbol{x}_2)$. For the gPC interpolation, we need 486 grid points for the non-nested sparse grids with sparseness level 2 based on the one-dimensional Gauss quadrature formula. We use sparseness level 2 because that the K–L expansion is a first-order polynomial with respect to the random variables.

In Figs. 10 and 11 we show the mean and the standard deviation along the center line $x = 0.5$. The statistics are computed by both direct Monte Carlo simulations and the gPC predictor model (see Eq. (18)). For Monte Carlo simulations, we sample the stochastic elliptic PDE directly; for the gPC predictor model, we first sample the stochastic elliptic PDE 486 (the number of sparse grid points) times to obtain the approximate gPC solution $\tilde{u}_p(\boldsymbol{x};\boldsymbol{Y})$, which is a second-order polynomial with respect to 10 random variables (see Eq. (16)), and then sample $\tilde{u}_p(\boldsymbol{x};\boldsymbol{Y})$ instead of the stochastic elliptic PDE to compute statistics. It can be seen that sampling the gPC solution $\tilde{u}_p(\boldsymbol{x};\boldsymbol{Y})$ 100,000 times provides a comparable accuracy with that given by sampling the stochastic PDE 100,000 times. However, the numerical cost is significantly different. The main numerical cost of both strategies comes from sampling the stochastic PDE. For the comparable accuracy, we only need to solve 486 deterministic PDEs for the gPC predictor model in contrast to solving 100,000 deterministic PDEs for the direct Monte Carlo method, which results in a speed up of $O(200)$. Since the gPC predictor model yields accurate statistics, we know that the predictor-corrector model (see Eq. (19)) will be effective to further refine the results, where the gPC solution is used a control variate for variance reduction.

6. Discussion

In this work, we have proposed and investigated a numerical methodology for elliptic problems with general (non-Gaussian) random inputs. We note that the methodology presented is a gen-

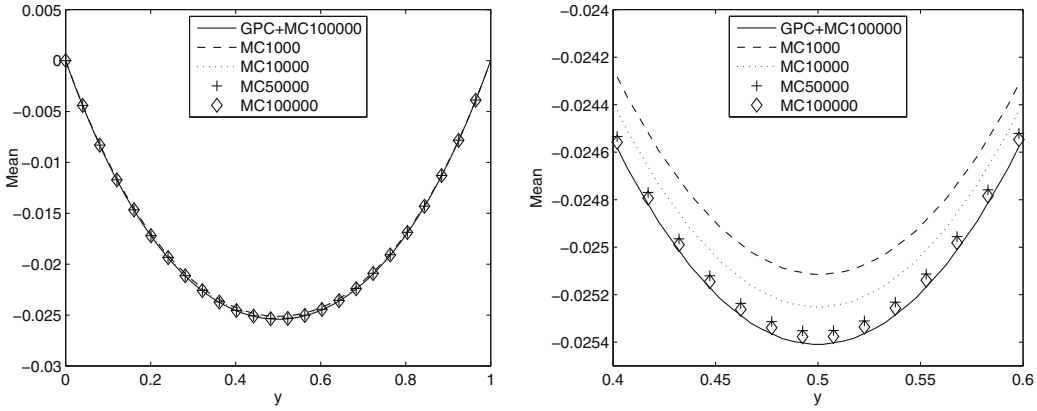

Fig. 10. Mean of $u(x;\omega)$ along the center line $x = 0.5$. Left: mean. Right: close-up view.

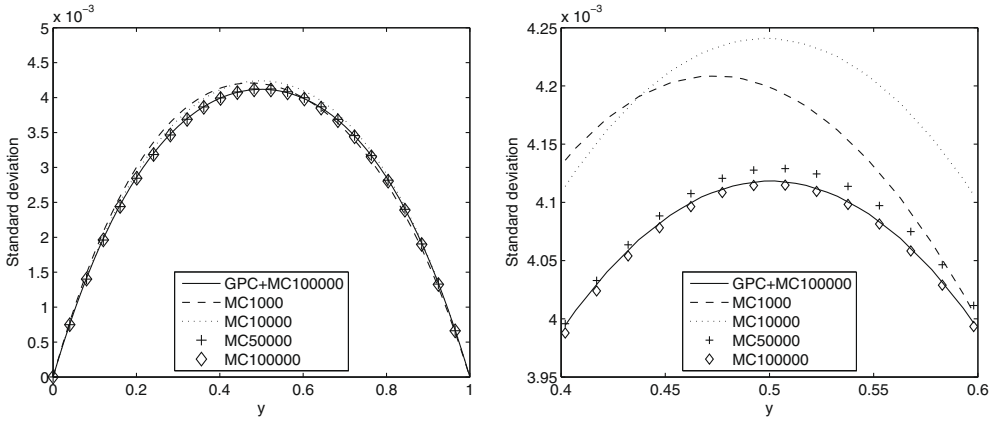

Fig. 11. Standard deviation of $u(x;\omega)$ along the center line $x = 0.5$. Left: standard deviation. Right: close-up view.

eral one, not restricted to the model problem used. The idea is based on the observation that the polynomial chaos method provides an approximate model of the original stochastic PDE while the Monte Carlo method only needs the outputs. Thus, we can 'feed' the Monte Carlo method using the polynomial chaos solution.

The Karhunen–Loève expansion, which is valid for any second-order random process, was employed to reduce the dimensionality of random inputs. To maintain the joint PDF of random variables in the Karhunen–Loève expansion, we considered a high-dimensional interpolation problem in the parametric space. By noting the analyticity of solution and the L_∞ convergence of polynomial interpolation in the parametric space, we implemented the polynomial chaos approximation based on an auxiliary PDF. In the post-processing stage, we considered two models. In the gPC predictor model, we computed all desired statistics by sampling the polynomial chaos solution with respect to the joint PDF instead of the auxiliary one. In the gPC predictor-corrector model, we used Monte Carlo methods to refine the statistics given by gPC predictor model, where the polynomial chaos solution served as a control variate for variance reduction to accelerate efficiently the convergence of the Monte Carlo method.

Acknowledgements

This work is supported by DOE, NSF, AFOSR and ONR.

Appendix A. Derivation of the correlation function of $R(x)$

Let $X_1 = R_\Gamma(x_1;\omega)$ and $X_2 = R_\Gamma(x_2;\omega)$, we first look at the generating function $g(\theta_1,\theta_2) = \mathbb{E}[e^{\theta_1 X_1+\theta_2 X_2}]$. Let $Y_{i,1} = G_i(x_1;\omega)$ and $Y_{i,2} = G_i(x_2;\omega)$. We know that $Y_{i,1}$ and $Y_{i,2}$ are normal random variables with covariance $K_G(|x_1-x_2|)$. It is easy to see

$$\begin{aligned} g(\theta_1,\theta_2) &= \mathbb{E}[e^{\theta_1 X_1+\theta_2 X_2}] = \prod_{i=1}^{2m}\mathbb{E}[e^{\frac{1}{2}\theta_1 G_i^2(x_1)+\frac{1}{2}\theta_2 G_i^2(x_2)}] \\ &= \prod_{i=1}^{2m}\frac{1}{2\pi\sqrt{1-K_G^2}} \\ &\quad\times\int_{\mathbb{R}^2} e^{\frac{1}{2}\theta_1 y_{i,1}+\frac{1}{2}\theta_2 y_{i,2}} e^{\frac{-1}{2(1-K_G^2)}(y_{i,1}^2+y_{i,2}^2-2K_G y_{i,1}y_{i,2})}\,dy_{i,1}y_{i,2} \\ &= \prod_{i=1}^{2m}((1-\theta_1)(1-\theta_2)-\theta_1\theta_2 K_G^2)^{-1/2} \\ &= ((1-\theta_1)(1-\theta_2)-\theta_1\theta_2 K_G^2)^{-m} \end{aligned} \tag{A.1}$$

We are now ready to compute the correlation function of $R_\Gamma(x;\omega)$

$$\begin{aligned} K_{R_\Gamma}(x_1,x_2) &= \frac{\mathbb{E}[(R_\Gamma(x_1)-\mathbb{E}[R_\Gamma](x_1))(R_\Gamma(x_2)-\mathbb{E}[R_\Gamma](x_2))]}{\sigma_{R_\Gamma}(x_1)\sigma_{R_\Gamma}(x_2)} \\ &= \frac{\mathbb{E}[(X_1-m)(X_2-m)]}{m} = \frac{\mathbb{E}[X_1X_2]-m^2}{m} \\ &= \frac{\frac{\partial^2 g}{\partial\theta_1\partial\theta_2}|_{\theta_1=\theta_2=0}-m^2}{m} = K_G^2(|x_1-x_2|). \end{aligned} \tag{A.2}$$

References

[1] M. Shinozuka, G. Deodatis, Simulation of stochastic processes by spectral representation, Appl. Mech. Rev. 44 (4) (1991) 191–203.
[2] M. Loeve, Probability Theory, fourth ed., Springer-Verlag, New York, 1977.
[3] B.A. Zeldin, P.D. Spanos, Random field simulation using wavelet bases, ASME J. Appl. Mech. 63 (4) (1996) 946–952.
[4] F.W. Elliott, D.J. Horntrop, A.J. Majda, A Fourier-Wavelet Monte Carlo method for fractal random fields, J. Comput. Phys. 132 (1997) 384–408.
[5] S. Sakamoto, R.G. Ghanem, Polynomial chaos decomposition for simulation of non-Gaussian non-stationary stochastic processes, ASCE J. Engrg. Mech. 128 (2) (2002) 190–200.
[6] B. Puig, J.L. Akian, Non-Gaussian simulation using Hermite polynomial expansion and maximum entropy principle, Probab. Engrg. Mech. 19 (2004) 293–305.
[7] K.K. Phoon, S.P. Huang, S.T. Quek, Simulation of strongly non-Gaussian processes using Karhunen–Loève expansion, Probab. Engrg. Mech. 20 (2005) 188–198.
[8] R.G. Ghanem, P. Spanos, Stochastic Finite Elements: A Spectral Approach, Springer-Verlag, New York, 1991.
[9] M.K. Deb, I. Babuška, J.T. Oden, Solution of stochastic partial differential equations using Galerkin finite element techniques, Comput. Methods Appl. Mech. Engrg. 190 (2001) 6359–6372.
[10] D. Xiu, G.E. Karniadakis, The Wiener–Askey polynomial chaos for stochastic differential equations, SIAM J. Sci. Comput. 24 (2) (2002) 619–644.
[11] O.P.L. Maitre, H.N. Njam, R.G. Ghanem, O.M. Knio, Uncertainty propagation using Wiener–Haar expansions, J. Comput. Phys. 197 (2004) 28–57.
[12] H.G. Matthies, A. Keese, Galerkin methods for linear and nonlinear elliptic stochastic partial differential equations, Comput. Methods Appl. Mech. Engrg. 194 (12-16) (1999) 1295–1331.
[13] P. Frauenfelder, C. Schwab, R.A. Todor, Finite elements for elliptic problems with stochastic coefficients, Comput. Methods Appl. Mech. Engrg. 194 (2005) 205–228.
[14] X. Wan, G.E. Karniadakis, An adaptive multi-element generalized polynomial chaos method for stochastic differential equations, J. Comput. Phys. 209 (2) (2005) 617–642.
[15] X. Wan, G.E. Karniadakis, Multi-element generalized polynomial chaos for arbitrary probability measures, SIAM J. Sci. Comput. 28 (3) (2006) 901–928.
[16] I. Babuška, F. Nobile, R. Tempone, A stochastic collocation method for elliptic partial differential equations with random input data, SIAM J. Numer. Anal. 45 (3) (2007) 1005–1034.
[17] K.E. Atkinson, The Numerical Solution of Integral Equations of the Second Kind, Cambridge University Press, 1997.
[18] C. Schwab, R.A. Todor, Karhunen–Loève approximation of random fields by generalized multipole methods, J. Comput. Phys. 217 (1) (2006) 100–122.
[19] X. Wan, G.E. Karniadakis, A sharp error estimate of the fast gauss transform, J. Comput. Phys. 219 (1) (2006) 7–12.
[20] B. Oksendal, Stochastic Differential Equations, Springer-Verlag, 1998.
[21] E. Parzen, On estimation of a probability density function and mode, Ann. Math. Stat. 33 (3) (1962) 1065–1076.
[22] A.J. Izenman, Recent developments in nonparametric density estimation, J. Amer. Stat. Assoc. 86 (413) (1991) 205–224.
[23] M.P. Wand, M.C. Jones, Kernel Smoothing, Chapman and Hall, 1995.
[24] G. Mastroianni, D. Occorsiol, Optimal systems of nodes for lagrange interpolation on bounded intervals. A survey, J. Comput. Appl. Math. 134 (2001) 325–341.
[25] E. Novak, K. Ritter, Simple cubature formulas with high polynomial exactness, Constr. Approx. 15 (1999) 499–522.
[26] R.A. Devore, G.G. Lorentz, Constructive Approximation, Springer-Verlag, Berlin, 1993.
[27] V. Barthelmann, E. Novak, K. Ritter, High dimensional polynomial interpolation on sparse grids, Adv. Comput. Math. 12 (2000) 273–288.
[28] F. Nobile, R. Tempone, C.G. Webster, A sparse grid stochastic collocation method for partial differential equations with random input data, SIAM J. Numer. Anal. 46 (5) (2008) 2309–2345.
[29] R.A. Todor, C. Schwab, Convergence rates for sparse chaos approximations of elliptic problems with stochastic coefficients, IMA J. Numer. Anal. 27 (2) (2007) 232–261.
[30] R.G. Ghanem, Stochastic finite elements for heterogeneous media with multiple random non-Gaussian properties, ASCE J. Engrg. Mech. 125 (1) (1999) 26–40.
[31] I. Babuška, R. Tempone, G.E. Zouraris, Galerkin finite element approximations of stochastic elliptic differential equations, SIAM J. Numer. Anal. 42 (2) (2004) 800–825.
[32] X. Wan, G.E. Karniadakis, Error control in multi-element generalized polynomial chaos method for elliptic problems with random coefficients, Commun. Comput. Phys. 5 (2–4) (2009) 793–820.
[33] W. Gautschi, On generating orthogonal polynomials, SIAM J. Sci. Stat. Comput. 3 (3) (1982) 289–317.
[34] L. Greengard, J. Strain, The fast Gauss transform, SIAM J. Sci. Stat. Comput. 12 (1) (1991) 79–94.
[35] J. Foo, X. Wan, G.E. Karniadakis, The multi-element probabilistic collocation method: error analysis and simulation, J. Comput. Phys. 227 (22) (2008) 9572–9595.